ORIGINAL RESEARCH

Insights into the bending effect in premixed turbulent combustion using the Flame Surface Density transport

Umair Ahmed[a], Nilanjan Chakraborty[a] and Markus Klein[b]

[a]School of Engineering, Newcastle University, Newcastle Upon Tyne NE1 7RU, UK

[b]Universität der Bundeswehr München, Werner Heisenberg Weg 39, D-85577 Neubiberg, Germany

ARTICLE HISTORY

Compiled January 31, 2019

ABSTRACT

The bending effect of turbulent flame speed variation (i.e. the deviation from the linear increase of flame speed with increasing turbulence intensity, with increasing root-mean-square turbulent velocity fluctuation, has been investigated based on a Direct Numerical Simulation (DNS) database of statistically planar turbulent premixed flames propagating into forced unburned gas turbulence. The validity of Damköhler's first hypothesis has been utilised to analyse the bending effect in terms of generalised Flame Surface Density (FSD) evolution. The volume-integrated value of the tangential strain rate term of the FSD transport equation remains positive, whereas the volume-integrated value of the curvature term assumes negative values. Under statistically stationary state, the positive value of the volume-integrated tangential strain rate term remains in equilibrium with the negative value of the volume-integrated curvature term. It has been found that the contribution of the normal strain rate to the flame surface area remains negative for small turbulence intensities, which eventually become positive for large turbulence intensities. This is a consequence of the change of collinear alignment of the reaction progress variable gradient from the most extensive principal strain rate direction to the direction of the eigenvector associated with the most compressive principal strain rate with increasing turbulence intensity. An increase in turbulence intensity increases the width

U. Ahmed. Email: umair.ahmed@newcastle.ac.uk. Corresponding author
N. Chakraborty. Email: nilanjan.chakraborty@newcastle.ac.uk
M. Klein. Email:markus.klein@unibw.de

of the probability density functions of flame curvature, and thereby increases the surface averaged curvature squared values. This eventually makes the FSD curvature term due to the tangential diffusion component of displacement speed as the major contributor to the negative contribution of the volume-integrated curvature term in the FSD transport equation for large turbulence intensities. However, the negative contribution of the volume-integrated FSD curvature term does not increase indefinitely with increasing turbulence intensity and the inner cut-off scale, which also limits the maximum possible value of the volume-integrated FSD strain rate term under statistically stationary state, governs the maximum possible destruction of flame surface area. It has been argued that the upper limits of the flame surface area generation and destruction are responsible for the bending effects in the variations of turbulent flame speed and flame surface area.

KEYWORDS

Turbulent flame speed, Flame surface area, tangential strain rate, normal strain rate, displacement speed, curvature

1. Introduction

Turbulent flame speed S_T is a quantity of fundamental interest in premixed turbulent combustion (Abdel-Gayed & Bradley, 1977; Bradley, 1992, 2002; Bray, 1990; Karpov & Sokolik, 1961; Lipatnikov & Chomiak, 2002, 2005; Peters, 2000). It has been experimentally observed (Abdel-Gayed et al., 1984; Abdel-Gayed & Bradley, 1977; Karpov & Sokolik, 1961) that the turbulent flame speed S_T increases at a higher rate with increasing root-mean square velocity fluctuation u' for small values of turbulence intensities u'/S_L (where S_L is the unstrained laminar burning velocity) than for large values of u'/S_L. This phenomenon is commonly referred to as the bending effect, which has been well documented in the existing literature (see review papers by Lipatnikov and Chomiak (2002, 2005)). The physical explanations for this bending effect are yet to be unambiguously identified in the existing literature. In order to discuss the available hypotheses (Abdel-Gayed et al., 1984; Bradley, 1992, 2002; Bray & Cant, 1991), which attempted to explain the bending effect, it is useful to define the turbulent flame speed S_T. The turbulent flame speed S_T is closely linked to the burning rate and is defined as:

$$S_T = \frac{1}{\rho_0 A_L} \int_V \dot{\omega} dV, \tag{1}$$

where ρ_0 is the unburned gas density, A_L is the projected flame area in the direction of mean flame propagation, $\dot{\omega}$ is the reaction rate of the reaction progress variable c which can be defined in terms of a suitably normalised scalar (e.g. mass fraction of a major reactant) such that it increases monotonically from 0 in the unburned gas to unity in the fully burned products. In this context, it is worth noting that Eq. 1 can be rewritten in terms of Reynolds-averaged/filtered reaction rate $\overline{\dot{\omega}}$ in the following manner as the volume-integrated total burning rate is independent of the averaging/filtering process:

$$S_T = \frac{1}{\rho_0 A_L} \int_V \overline{\dot{\omega}} dV, \tag{2}$$

According to the Flame Surface Density (FSD) based reaction rate closure one obtains (Boger et al., 1998; Trouvé & Poinsot, 1994):

$$\overline{\dot{\omega} + \nabla . \left(\rho D \nabla c\right)} = \overline{\left(\rho S_d\right)}_s \Sigma_{gen}, \tag{3}$$

where $S_d = |\nabla c|^{-1} \left(Dc/Dt\right)$ is the local displacement speed, $\Sigma_{gen} = \overline{|\nabla c|}$ is the generalised FSD and $\overline{\left(Q\right)}_s = \overline{Q|\nabla c|}/\Sigma_{gen}$ is the surface-averaged/filtered value of a general quantity Q (Boger et al., 1998; Trouvé & Poinsot, 1994). Using Eq. 3 it is possible to express S_T as:

$$S_T = \frac{1}{\rho_0 A_L} \int_V \overline{\dot{\omega}} = \frac{1}{\rho_0 A_L} \int_V \overline{\dot{\omega} + \nabla . \left(\rho D \nabla c\right)} dV = \frac{1}{\rho_0 A_L} \int_V \overline{\left(\rho S_d\right)}_s \Sigma_{gen} dV. \tag{4}$$

Equation 4 is obtained because $\int_V \overline{\nabla . \left(\rho D \nabla c\right)} dV = \int_V \nabla . \left(\rho D \nabla c\right) dV = 0$ according to the divergence theorem. Subject to the assumption of $\overline{\left(\rho S_d\right)}_s \approx \rho_0 S_L$, often made in the existing literature for unity Lewis number flames (Boger et al., 1998; Hawkes &

Cant, 2001)), one gets:

$$S_T = \frac{S_L}{A_L}\int_V \Sigma_{gen} dV = S_L \frac{A_T}{A_L} \text{ or } \frac{S_T}{S_L} = \frac{A_T}{A_L}, \tag{5}$$

where $A_T = \int_V \Sigma_{gen} dV = \int_V |\nabla c| dV$ is the turbulent flame area. Equation 5 provides the well-known Damköhler's first hypothesis (Damköhler, 1940). However, in reality, the assumption $\overline{(\rho S_d)}_s \approx \rho_0 S_L$ might not be valid (Chakraborty et al., 2019; Chakraborty & Cant, 2007, 2011; Sabelnikov et al., 2017) under general conditions, and the stretch rate effects on displacement speed due to turbulence act to modify $\overline{(\rho S_d)}_s$ in comparison to $\rho_0 S_L$. This mechanism becomes increasingly strong with increasing u'/S_L and may contribute to the bending effect. However, it has recently been shown by Nivarti and Cant (2017a) that the Damköhler's first hypothesis (i.e. $S_T/S_L = A_T/A_L$) remains valid even for large turbulence intensities for statistically planar flames and possible explanations for this observation have been provided by Chakraborty et al. (2019). The reasonable agreement between S_T/S_L and A_T/A_L in statistically planar flames in the presence of bending suggests that the evolution of the generalised FSD Σ_{gen} plays a pivotal role in this process, due to its association with the flame surface area A_T. Recently, Yu et al. (2015) analysed the bending phenomenon from the point of view of the role of molecular diffusion using G-equation Direct Numerical Simulation (DNS) without heat release, while Yu and Lipatnikov (2017) analysed the same phenomenon using the DNS of the propagation of a reaction wave in forced, constant-density, homogeneous, isotropic turbulence.

The molecular diffusion effects are expected to influence the flame surface area through the displacement speed $S_d = \left[\dot{\omega} + \nabla.\left(\rho D \nabla c\right)\right]/\rho|\nabla c|$ dependence of the FSD transport equation (Chakraborty & Cant, 2007, 2009). Thus, the present analysis attempts to explain the bending effect from the point of view of flame surface area generation and destruction using the generalised FSD transport. This has been achieved by considering a three-dimensional DNS database of freely propagating statistically planar unity Lewis number turbulent premixed flames under forced stationary turbulence in the unburned gas ahead of the flame. The main objectives of this analysis are:

(1) To explain the bending effect in the turbulent flame speed variation with turbulence intensity from the point of view of FSD transport.

(2) To demonstrate the physical mechanisms which lead to the bending effect.

The mathematical background related to the generalised FSD transport will be provided in the next section. The numerical implementation pertaining to the DNS database considered here will be provided in the following section. This will be followed up by the presentation of results and their discussion. The main findings will be summarised and conclusions will be drawn in the final section of this paper.

2. Mathematical Background

The transport equation of the generalised FSD Σ_{gen} is given by (Candel & Poinsot, 1990; Chakraborty & Cant, 2007, 2009; Hawkes & Cant, 2001; Pope, 1988):

$$\frac{\partial \Sigma_{gen}}{\partial t} + \underbrace{\frac{\partial \left(\widetilde{u}_j \Sigma_{gen}\right)}{\partial x_j}}_{C_1-\text{convection}} = \underbrace{-\frac{\partial \left\{ \left[\overline{(u_k)}_s - \widetilde{u}_k \right] \Sigma_{gen} \right\}}{\partial x_k}}_{T_1-\text{turbulent transport}} + \underbrace{\overline{\left(\left(\delta_{ij} - N_i N_j\right) \frac{\partial u_i}{\partial x_j} \right)}_s \Sigma_{gen}}_{T_2-\text{strain rate}}$$
$$\underbrace{-\frac{\partial \left[\overline{(S_d N_k)}_s \Sigma_{gen} \right]}{\partial x_k}}_{T_3-\text{propagation}} + \underbrace{\overline{\left(S_d \frac{\partial N_i}{\partial x_i} \right)}_s \Sigma_{gen}}_{T_4-\text{curvature}}, \tag{6}$$

where $\overrightarrow{N} = -\nabla c/|\nabla c|$ is the local flame normal vector, $\kappa_m = \nabla.\overrightarrow{N}/2$ is the local flame curvature and $\widetilde{Q} = \overline{\rho Q}/\overline{\rho}$ is the Favre-average/filtered value of a general quantity Q. The term C_1 is the mean/resolved convection term, whereas T_1 is the turbulent transport term. The terms T_2, T_3 and T_4 on the right hand side of Eq. 6 arise due to tangential strain rate, flame propagation and flame curvature, respectively and these terms are thus referred to as the tangential strain rate term, FSD propagation term and FSD curvature term, respectively. It is worth noting that C_1, T_1, and T_3 are not source/sink terms because on volume integration these terms vanish according to the divergence theorem:

$$C_{1V} = \int_V \frac{\partial\left(\widetilde{u}_j \Sigma_{gen}\right)}{\partial x_j} dV = 0; \qquad T_{1V} = \int_V -\frac{\partial\left\{\left[\overline{(u_k)_s} - \widetilde{u}_k\right]\Sigma_{gen}\right\}}{\partial x_k} dV = 0;$$
$$T_{3V} = \int_V -\frac{\partial\left[\overline{(S_d N_k)_s}\Sigma_{gen}\right]}{\partial x_k} dV = 0. \tag{7}$$

This suggests on volume-integrating Eq. 6 one obtains:

$$\frac{\partial A_T}{\partial t} = \underbrace{\frac{\partial}{\partial t}\int_V \Sigma_{gen} dV}_{T_{RV}} = \int_V \frac{\partial \Sigma_{gen}}{\partial t} dV = \int_V T_2 dV + \int_V T_4 dV. \tag{8}$$

Under a statistically stationary state, the left hand side of Eq. 8 vanishes and thus $\int_V T_2 dV$ and $\int_V T_4 dV$ determine the flame surface area evolution. In order to understand the behaviour of $\int_V T_2 dV$ and $\int_V T_4 dV$, it is worthwhile to consider different components of the tangential strain rate and curvature terms.

The tangential strain rate term T_2 can be split as (Chakraborty & Cant, 2011; Katragadda et al., 2011):

$$T_2 = T_{21} + T_{22} = \overline{\left(\frac{\partial u_i}{\partial x_i}\right)_s}\Sigma_{gen} - \overline{\left(N_i N_j \frac{\partial u_i}{\partial x_j}\right)_s}\Sigma_{gen}, \tag{9}$$

where T_{21} arises due to dilatation rate and will henceforth be referred to as the dilatation rate term, whereas T_{22} arises due to the negative of normal strain rate and therefore will be referred to as the normal strain rate contribution. The value of $T_{2V} = \int_V T_2 dV$ depends on the behaviours of $T_{21V} = \int_V T_{21} dV$ and $T_{22V} = \int_V T_{22} dV$.

Using different components of displacement speed, it is possible to split the FSD curvature term T_4 as (Chakraborty & Cant, 2007, 2009, 2011; Katragadda et al., 2014):

$$T_4 = T_{41} + T_{42} = 2\overline{\left[\left(S_r + S_n\right)\kappa_m\right]_s}\Sigma_{gen} - 4\overline{\left(D\kappa_m^2\right)_s}\Sigma_{gen}, \tag{10}$$

where $S_r = \dot{\omega}/\rho|\nabla c|$ and $S_n = \overrightarrow{N}.\nabla\left(\rho D\overrightarrow{N}.\nabla c\right)/\rho|\nabla c|$ are the reaction and normal diffusion components of displacement speed (Echekki & Chen, 1999; Peters et al.,

1998). The term T_{42} originates due to molecular diffusion in the flame tangential direction. Equation 10 suggests that $T_{4V} = \int_V T_4 dV$ depends on the behaviours of $T_{41V} = \int_V T_{41} dV$ and $T_{42V} = \int_V T_{42} dV$. The statistical behaviours of T_{2V}, T_{21V}, T_{22V}, T_{4V}, T_{41V} and T_{42V} is discussed in detail in Section 4 of this paper.

3. Numerical Implementation

A well-known DNS code SENGA (Jenkins & Cant, 1999) has been used for the simulations considered in this work. The conservation equations of mass, momentum, energy and species are solved in non-dimensional form in SENGA. All the spatial derivatives for the internal grid points have been evaluated using a 10^{th} order central difference scheme and the order of differentiation gradually decreases to a 2^{nd} order one-sided scheme at the non-periodic boundaries. The time-advancement has been carried out by a 3^{rd} order explicit Runge-Kutta scheme (Wray, 1990). The simulations for the statistically planar premixed flames have been conducted in an inlet-outlet configuration where the inlet and outlet boundaries are specified in the direction of mean flame propagation. The transverse boundaries have been considered to be periodic. The outflow boundary is taken to be partially non-reflecting and specified according to the Navier-Stokes Characteristic Boundary Conditions (NSCBC) technique (Poinsot & Lele, 1992). The mean inlet velocity U_{mean} has been gradually modified to match the turbulent flame speed so that the flame remains stationary in the statistical sense within the computational domain. The simulation domain, the size of the uniform Cartesian grid used for discretising the domain along with the inlet values of root-mean-square turbulent velocity fluctuation normalised by the unstrained laminar burning velocity u'/S_L, integral length scale to thermal flame thickness ratio l/δ_{th}, Damköhler number $Da = lS_L/u'\delta_{th}$, Karlovitz number $Ka = (u'/S_L)^{3/2} (l/\delta_{th})^{-1/2}$ and the heat release parameter $\tau = (T_{ad} - T_0)/T_0$ are listed in Table 1; where $\delta_{th} = (T_{ad} - T_0)/\max|\nabla T|_L$ is the thermal flame thickness with T, T_0 and T_{ad} being the dimensional temperature, unburned gas temperature and the adiabatic flame temperature, respectively. The grid spacing ensures at least 10 grid points within δ_{th} and 1.5 grid points within the Kolmogorov length scale η. A recently proposed modi-

	u'/S_L	l/δ_{th}	Da	Ka	τ	Domain Size	Grid Size
Case-A	1.0	3.0	3.0	0.58	4.5	$79.5\delta_{th} \times (39.8\delta_{th})^2$	$800 \times (400)^2$
Case-B	3.0	3.0	1.0	3.0	4.5	$79.5\delta_{th} \times (39.8\delta_{th})^2$	$800 \times (400)^2$
Case-C	5.0	3.0	0.6	6.5	4.5	$79.5\delta_{th} \times (39.8\delta_{th})^2$	$800 \times (400)^2$
Case-D	7.5	3.0	0.4	11.9	4.5	$79.5\delta_{th} \times (39.8\delta_{th})^2$	$800 \times (400)^2$
Case-E	10.0	3.0	0.3	18.3	4.5	$79.5\delta_{th} \times (39.8\delta_{th})^2$	$800 \times (400)^2$

Table 1.: Simulation parameters for all the cases considered.

fied bandwidth filtered forcing method (Klein et al., 2017) in physical space has been used for the unburned gas ahead of the flame, which not only maintains the prescribed turbulence intensity u'/S_L but also provides the required integral length scale to flame thickness ratio l/δ_{th}, where l is calculated using turbulent kinetic energy and its dissipation rate evaluated over the whole domain. The u'/S_L and l/δ_{th} values considered here are shown on the regime diagram by Peters (2000) in figure 1, which suggests that these cases span from the wrinkled flamelet regime close to the broken reaction zones regime. For the purpose of computational economy, the chemical mechanism is simplified here by a single-step Arrhenius mechanism. The Lewis number of all the species is taken to be unity and the gaseous mixture is considered to obey the ideal gas law. Standard values are taken for Prandtl number (i.e. $Pr = 0.7$), Zel'dovich number (i.e. $\beta_z = T_{ac}\left(T_{ad} - T_0\right)/T_{ad}^2 = 6.0$) with T_{ac} being the activation temperature) and the ratio of specific heats (i.e. $\gamma = 1.4$). All the simulations listed in Table 1 have been continued until the turbulent kinetic energy and integral length scale attain the desired values after initial transience have decayed and also the turbulent flame speed S_T and flame surface area A_T settle to statistically stationary values. Interested readers are referred to Klein et al. (2017) and references therein for further information and the methodology associated with calibration of unburned gas forcing. The simulation time remains greater than one flow through time (i.e. $t_{sim} > L_x/U_{mean}$) and at least 10 eddy turn over times (i.e. $t_{sim} > 10l/u'$) for all cases.

For the purpose of Reynolds/Favre averaging, the quantities of interest are ensemble averaged in the homogeneous directions, which are the transverse directions normal to the mean flame propagation direction in the current configuration following several previous analyses (Veynante et al., 1997; Zhang & Rutland, 1995). In statistically planar flames the Favre-averaged reaction progress variable $\widetilde{c}$ remains a unique function

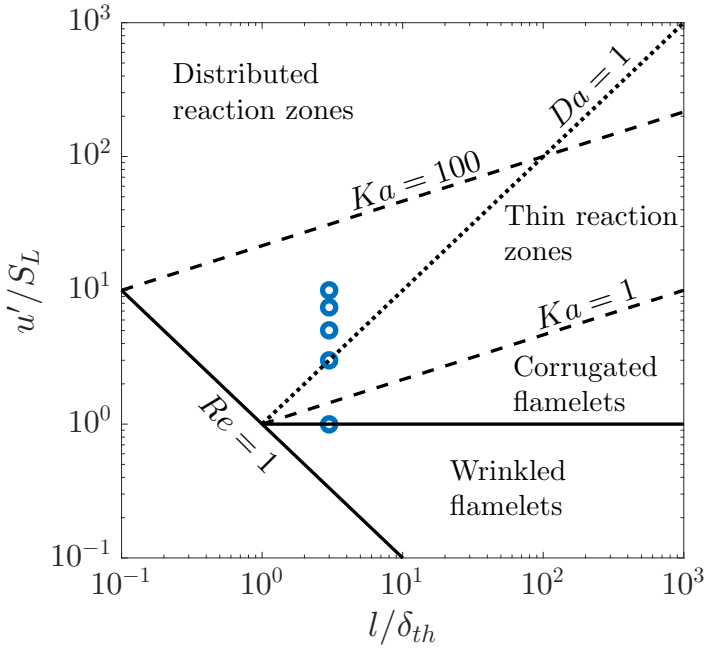

Figure 1.: The cases considered here on the regime diagram by Peters (2000)

of the coordinate in the direction of mean flame propagation (i.e. x_1-direction).

4. Results and Discussion

The instantaneous views of the reaction progress isosurfaces for $c = 0.1$, 0.5 and 0.9 are shown in Fig. 2 for all cases considered here, while Fig. 3 shows the contours of the reaction progress variable in the $x - y$ mid-plane of the computational domain for the same cases. It can be seen from Figs. 2 and 3 that the isosurfaces are wrinkled by turbulent motion in the cases with small Karlovitz number (i.e. $Ka < 1$ as in case-A) but they remain parallel to each other. However, this behaviour changes significantly for cases with high Karlovitz number (i.e. $Ka > 1$ as in case-B) where the c isosurfaces on the unburned gas side of the flame representing the preheat zone are more wrinkled than the isosurfaces towards the burned gas side of the flame front. The energetic turbulent eddies enter into the flame and increasingly disturb the thermo-chemical structure of the flame with increasing Karlovitz number Ka. It is evident from Figs. 2 and 3 that the extent of flame wrinkling generally increases with increasing u'/S_L, which can be quantified with the help of the normalised flame surface area A_T/A_L.

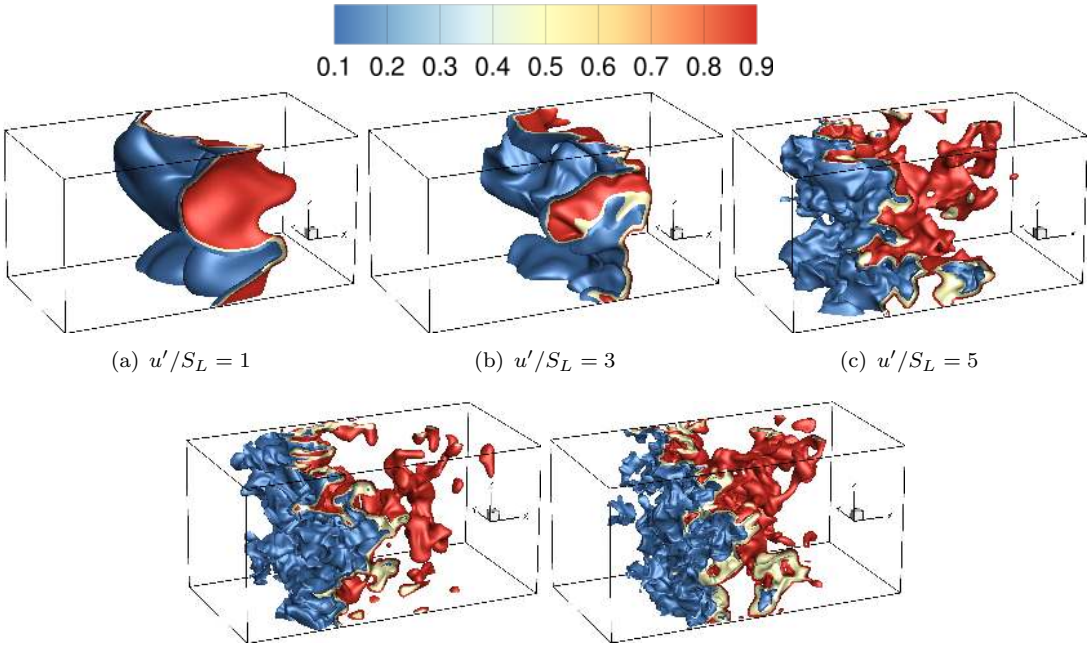

(a) $u'/S_L = 1$ (b) $u'/S_L = 3$ (c) $u'/S_L = 5$

(d) $u'/S_L = 7.5$ (e) $u'/S_L = 10$

Figure 2.: Iso-surfaces of the progress variable for all the cases investigated.

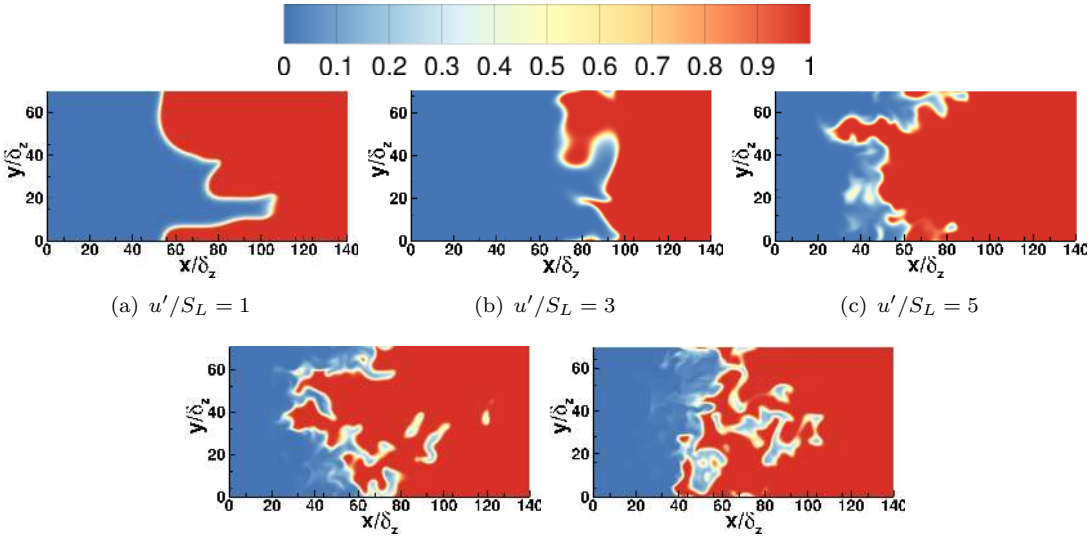

(a) $u'/S_L = 1$ (b) $u'/S_L = 3$ (c) $u'/S_L = 5$

(d) $u'/S_L = 7.5$ (e) $u'/S_L = 10$

Figure 3.: Contours of the progress variable recorded at the $x-y$ mid-plane for all the cases investigated.

The variation of A_T/A_L with u'/S_L is shown in Fig. 4a along with the corresponding values of S_T/S_L. Figure 4a suggests that S_T/S_L remains sufficiently close to A_T/A_L even for high values of u'/S_L. This suggests that Damköhler's first hypothesis (i.e. $S_T/S_L \approx A_T/A_L$) remains reasonably valid for statistically planar turbulent premixed flames (but not necessarily for flames characterized by a curved mean flame geometry, see Chakraborty et al. (2019)), which is consistent with previous findings of Nivarti and Cant (2017a). Note that the simulations performed in this work are different from those of Nivarti and Cant (2017a). In the current simulations the turbulence has been forced upstream of the flame, which ensures the required levels of turbulence and length scale ahead of the flame. In the case of Nivarti and Cant (2017a) no forcing is employed and the turbulence decays which leads to lower values of turbulence encountered by the flame as explained in table 1 of Nivarti and Cant (2017a). Figure 4a shows that both A_T/A_L and S_T/S_L increase with u'/S_L for small values of turbulence intensity but the rates of augmentation of A_T/A_L and S_T/S_L with increasing u'/S_L drop for large values of turbulence intensity, and at some stage both A_T/A_L and S_T/S_L become weak functions of u'/S_L. It can be seen from Fig. 4b that the value of $\overline{(\rho S_d)}_{sV}/\rho_0 S_L = \int_V (\dot{\omega} + \nabla.(\rho D \nabla c))\, dV / \int_V \rho_0 S_L |\nabla c| dV$ remains sufficiently close to unity, which ensures $S_T/S_L \approx A_T/A_L$ for the statistically planar flames considered here. However, it does not mean that locally $\overline{(\rho S_d)}_s$ remains equal to $\rho_0 S_L$ in these flames (not shown here) and interested readers are referred to (Chakraborty et al., 2019) for the explanations behind $\overline{(\rho S_d)}_{sV}/\rho_0 S_L \approx 1.0$ in statistically planar flames.

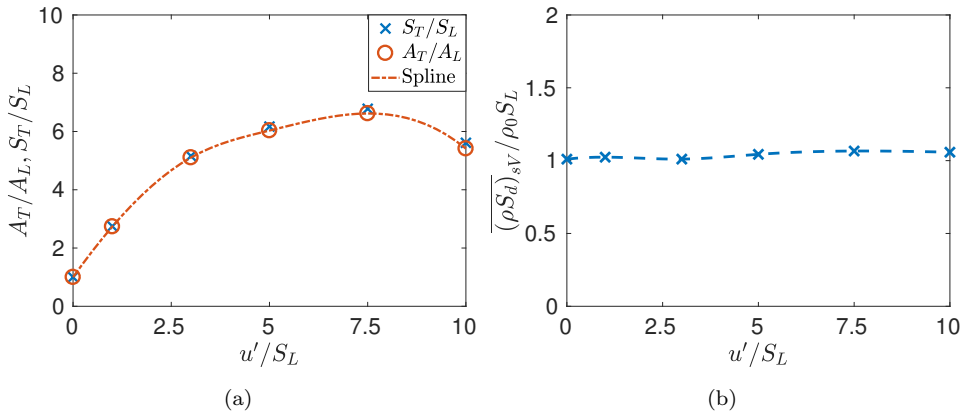

(a) (b)

Figure 4.: Variations of (a) A_T/A_L and S_T/S_L, and (b) $\overline{(\rho S_d)}_{sV}/\rho_0 S_L = \int_V (\dot{\omega} + \nabla(\rho D \nabla c) dV / \int_V \rho_0 S_L |\nabla c|$ with u'/S_L for all cases considered.

Figure 4a indicates that bending can be seen for both A_T/A_L and S_T/S_L variations with u'/S_L for the cases considered here. The bending effects for both A_T/A_L and S_T/S_L and the validity of Damköhler's first hypothesis indicate that the physical mechanisms, which are responsible for the bending effect in the A_T/A_L variation, lead to the bending effect for the normalised turbulent flame speed S_T/S_L variation. Thus, the following analysis will focus on the generalised FSD transport and statistical behaviours of C_V, T_{1V}, T_{2V}, T_{3V} and T_{4V}.

The validity of Damköhler's first hypothesis for unity Lewis number statistically planar premixed flames for large values of Karlovitz number (i.e. $Ka > 1$) within the thin reaction zones regime is consistent with several previous analyses (Aspden et al., 2011; Nivarti & Cant, 2017a). A recent analysis by Chakraborty et al. (2019) explained why Damköhler's first hypothesis remains valid for unity Lewis number statistically planar flames even for large values of Karlovitz number and thus it is not repeated here. Chatakonda et al. (2013) considered simultaneous validity of Damköhler's first and second hypotheses under low Damköhler number (and high Karlovitz number) conditions, whereas a recent analysis by Nivarti and Cant (2017b) suggested that Damköhler's second hypothesis does not necessarily hold for all conditions for $Ka > 1$. While the validity of Damköhlers second hypothesis and its possible overlap with the first hypothesis is an active area of research, it is not the focus of the current analysis and thus will not be elaborated in this work.

The variations of normalised T_{RV}, $(-C_V)$, T_{1V}, T_{2V} , T_{3V} and T_{4V} (i.e. $[T_{RV}$, $(-C_V)$, T_{1V} , T_{2V}, T_{3V} and $T_{4V}]\times\delta_{th}/(A_L S_L)$) with u'/S_L are shown in Fig 5 which shows that the contributions of $(-C_V)$, T_{1V} and T_{3V} remain vanishingly small in comparison to T_{2V} and T_{4V}. Furthermore, the contributions of volume-integrated tangential strain rate and curvature terms (i.e. T_{2V} and T_{4V}) remain positive and negative, respectively and they cancel each other, which can be substantiated from the vanishingly small values of T_{RV}. This further confirms the statistically stationary nature of the flames considered in this work. It can further be seen from Fig. 5 that the increase in the magnitudes of T_{2V} and T_{4V} with increasing u'/S_L are also non-linear in nature and both T_{2V} and T_{4V} do not change rapidly for large values of u'/S_L. In order to explain this behaviour it is instructive to examine the components of T_{2V} and T_{4V}.

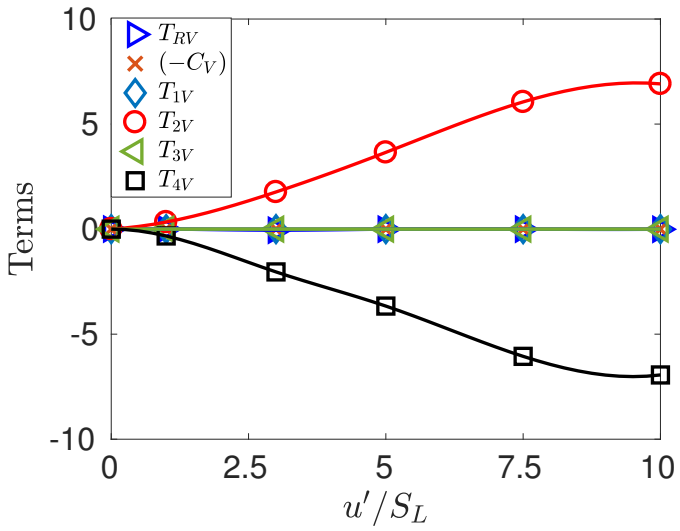

Figure 5.: Variations of $[T_{RV}, (-C_V), T_{1V}, T_{2V}, T_{3V}$ and $T_{4V}] \times \delta_{th}/(A_L S_L)$ with u'/S_L for all cases considered.

The variations of normalised T_{2V}, T_{21V} and T_{22V} (i.e. [T_{2V}, T_{21V} and T_{22V}] $\times \delta_{th}/(A_L S_L)$) with u'/S_L are shown in Fig. 6. Figure 6 shows that the volume-integrated dilatation rate term T_{21V} remains positive as the dilatation rate $\partial u_j/\partial x_j$ assumes predominantly positive values within the flame. The dilatation rate $\partial u_j/\partial x_j$ in premixed turbulent flames is principally determined by thermo-chemistry and thus the magnitude of T_{21V}/A_T, representing the ratio of the volume-integrated dilatation rate term and volume-integrated FSD, do not change significantly with the variation of turbulence intensity u'/S_L except for high values of u'/S_L where a marginal decrease in T_{21V}/A_T has been obtained (not shown here). Thus, the variation of T_{21V} with u'/S_L also shows bending, as can be seen from Fig. 6. For the cases considered here, l/δ_{th} is kept unaltered and thus an increase in u'/S_L amounts to an increase in Karlovitz number $Ka = (u'/S_L)^{3/2}(l/\delta_{th})^{-1/2}$ (see Fig. 1). Thus, the cases with high u'/S_L represent high Karlovitz number combustion where turbulent eddies penetrate into the flame and perturb thermo-chemical processes within the flame in such a manner that the dilatation rate magnitude gets adversely affected (Wacks et al., 2016). This leads to a marginal decrease in the magnitude of T_{21V}/A_T for high u'/S_L cases (not shown here).

The contribution of T_{22V} remains negative for small values of u'/S_L but it becomes positive for large values of u'/S_L . This can be explained as follows. The term T_{22} can

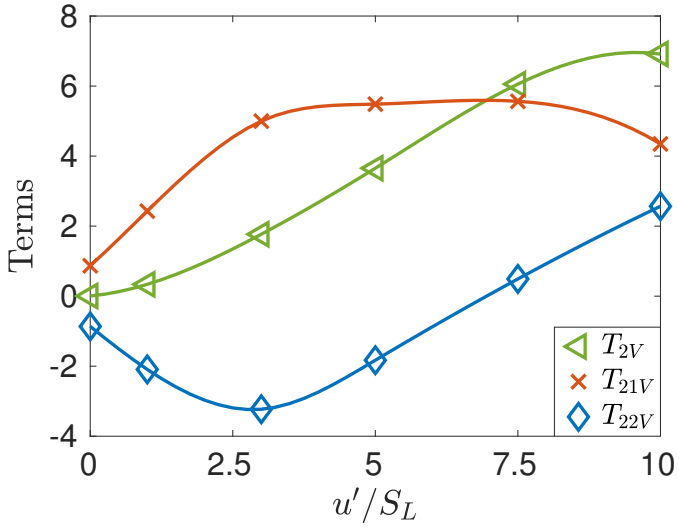

Figure 6.: Variations of $[T_{2V}$, T_{21V} and $T_{22V}]$ $\times\delta_{th}/(A_L S_L)$ with u'/S_L for all cases considered.

be expressed as: $T_{22} = -\overline{(e_\alpha \cos^2\theta_\alpha + e_\beta \cos^2\theta_\beta + e_\gamma \cos^2\theta_\gamma)\,|\nabla c|}$ (Katragadda et al., 2011; Sellmann et al., 2017) where e_α, e_β and e_γ are the most extensive, intermediate and the most compressive principal strain rates, respectively. Here, θ_α, θ_β and θ_γ are the angles between ∇c and the eigenvectors associated with e_α, e_β and e_γ , respectively. It has been discussed elsewhere (Ahmed et al., 2014; Chakraborty et al., 2009; Chakraborty & Swaminathan, 2007; Kim & Pitsch, 2007) that ∇c preferentially aligns collinearly with the eigenvector associated with e_α (i.e. high probability of obtaining $\cos^2\theta_\alpha \approx 1.0$) when the straining due to flame normal acceleration dominates over the turbulent straining, which is quantified as $\tau Da = \tau l S_L/u'\delta_{th} >> 1$ (Chakraborty & Swaminathan, 2007). This leads to negative values of T_{22} for small values of u'/S_L. By contrast, a preferential alignment between ∇c and the eigenvector associated with e_γ (i.e. high probability of obtaining $\cos^2\theta_\gamma \approx 1.0$) has been obtained similar to passive scalar mixing when turbulent straining dominates over the strain rate induced by flame normal acceleration, which is quantified by $\tau Da = \tau l S_L/u'\delta_{th} < 1$ (Chakraborty & Swaminathan, 2007) and leads to positive values of T_{22V}. In the current analysis, all cases have same values of l/δ_{th} and τ and thus an increase in u'/S_L leads to a decrease in τDa. Thus, the extent of alignment of ∇c with the eigenvector associated with $e_\alpha(e_\gamma)$ decreases (increases) with increasing u'/S_L . This can be substantiated from the probability density functions (PDFs) of $|\cos\theta_\alpha|$, $|\cos\theta_\beta|$ and $|\cos\theta_\gamma|$ in Fig. 7,

which shows that the probability of finding $|\cos\theta_\alpha| = 1.0$ is prevalent for small values of u'/S_L (e.g. $u'/S_L = 1.0$ and 3.0 cases), whereas a prevalence of $|\cos\theta_\gamma| = 1.0$ is observed for high values of u'/S_L (e.g. $u'/S_L = 10.0$ case). For the cases where $\tau Da \approx 1.0$ (e.g. $u'/S_L = 7.5$ case) the predominance of $|\cos\theta_\gamma| = 1.0$ is observed for both the unburned and burned gas side of the flame where the effects of heat release are weak. However, the probability of $|\cos\theta_\alpha| = 1.0$ is greater than finding perfect alignment with the eigenvectors associated with e_β and e_γ in the middle of the flame where the heat release effects are strong for the cases with $\tau Da \approx 1.0$ (e.g. $u'/S_L = 7.5$ case). It should be noted here that accounting for the changes in the relative alignment of the scalar gradient and the strain rate eigenvectors in modelling stratigies generally improves the model predictions as demonstrated in several previous a posteriori model assesments (Ahmed & Prosser, 2016, 2018; Butz et al., 2015; Dong et al., 2013).

The variations of normalised curvature terms T_{4V}, T_{41V} and T_{42V} $\times\delta_{th}/(A_L S_L)$) with u'/S_L are shown Fig. 8. It can be seen that both T_{41V} and T_{42V} assume negative values for all turbulence intensities considered here. The curvature term due to tangential diffusion component of displacement speed T_{42} is deterministically negative and thus T_{42V} assumes negative values for all cases considered here. For small values of u'/S_L the magnitudes of T_{41V} and T_{42V} remain comparable but the magnitude of T_{42V} supersedes that of T_{41V} for large values of u'/S_L . It has already been discussed that an increase in u'/S_L leads to increases in Karlovitz number Ka for the database considered in the current work. It has been demonstrated by Peters (2000) based on scaling arguments that T_{42} is expected to dominate over T_{41} for $Ka >> 1$, which has also been confirmed using previous DNS data (Chakraborty et al., 2007; Hawkes & Chen, 2005; Katragadda et al., 2014). It has been demonstrated and explained elsewhere (Chakraborty & Cant, 2004, 2005; Chakraborty & Klein, 2008a) that $(S_r + S_n)$ and κ_m remain weakly correlated for unity Lewis number flames, $|\nabla c|$ and κ_m also remain weakly correlated in these flames. The same is true for the flames considered here and this can be confirmed from Fig. 9 where the correlation coefficients between $(S_r + S_n)$ and κ_m (denoted by p_1), and between $|\nabla c|$ and κ_m (denoted by p_2) for different values of c across the flame are shown. Interested readers are referred to (Chakraborty & Cant, 2004, 2005) and (Chakraborty & Klein, 2008a) for physical

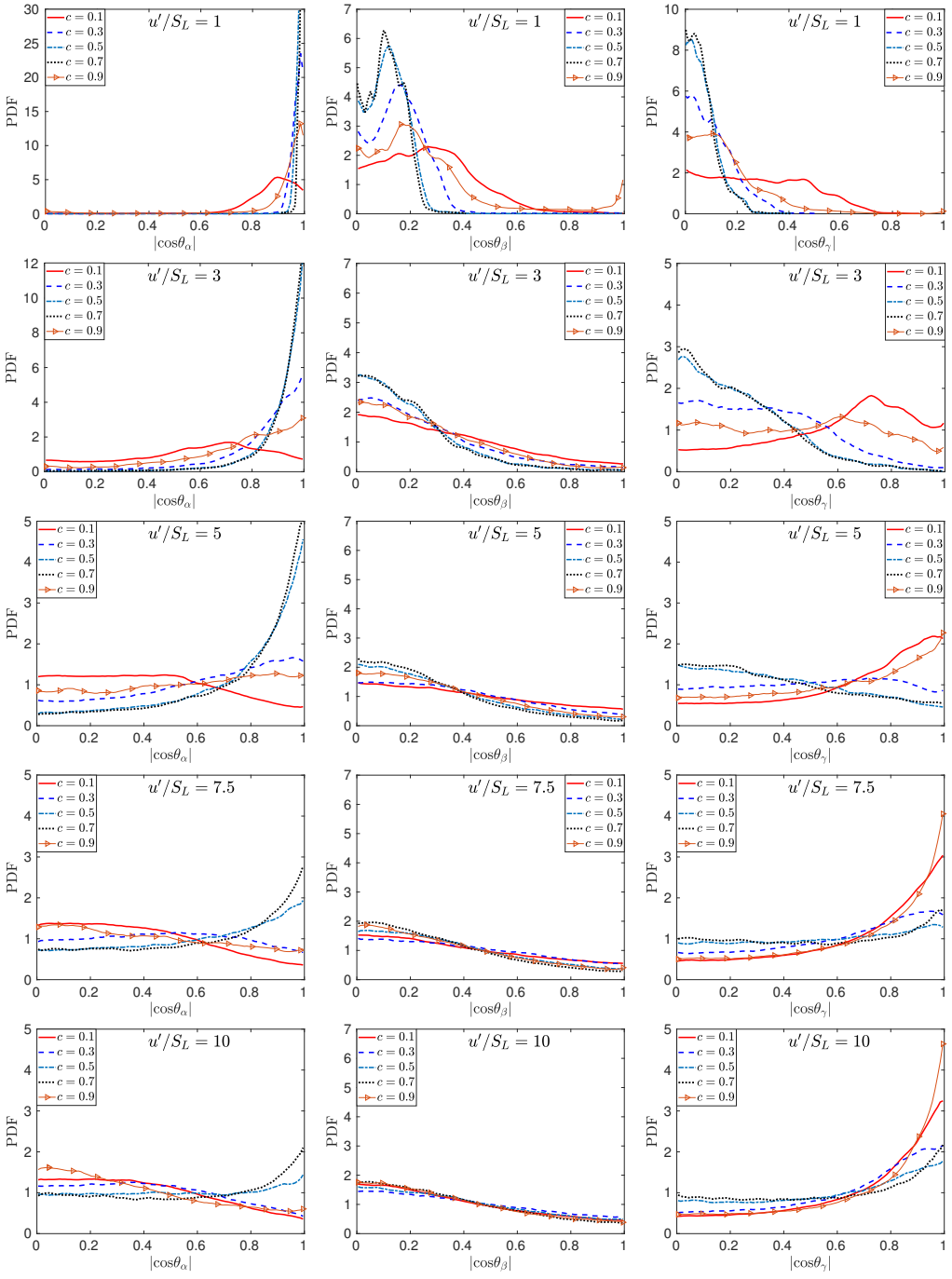

Figure 7.: PDFs of $|\cos\theta_\alpha|$, $|\cos\theta_\beta|$, $|\cos\theta_\gamma|$ for different c values across the flame for all cases considered.

explanations for the observed $(S_r + S_n) - \kappa_m$ and $|\nabla c| - \kappa_m$ correlations. The net effect of the weak correlations of $(S_r + S_n)$ and $|\nabla c|$ with κ_m leads to small negative values of T_{41V} for the cases considered here. The magnitude of T_{42V} increases with increasing u'/S_L before becoming insensitive to the variations of turbulence intensity

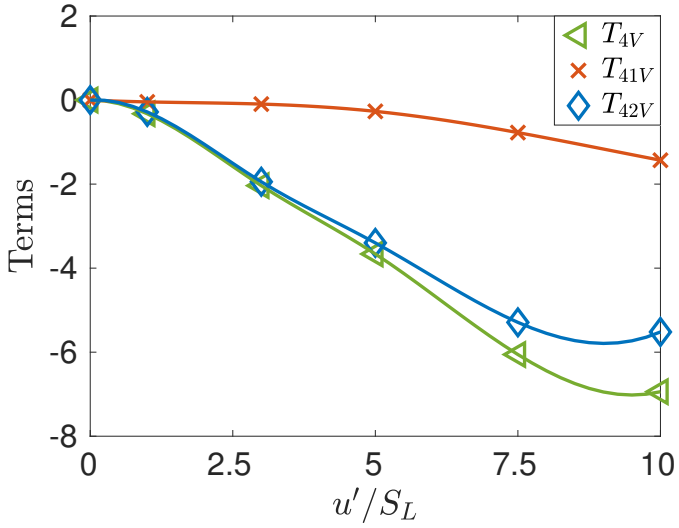

Figure 8.: Variations of [T_{4V}, T_{41V} and T_{42V}] $\times\delta_{th}/(A_L S_L)$ with u'/S_L for all cases considered.

for large values of u'/S_L.

In order to understand this behaviour it is worthwhile to look into the PDFs of curvature κ_m for different c values across the flame, which are presented in Fig. 10 for the cases considered in this work. Figure 10 shows that the mean value of κ_m remains negligible for the statistically planar flames considered here but the width of the PDF increases with increasing u'/S_L suggesting an increase in κ_m^2 as well. However, the increase in κ_m^2 does not happen indefinitely. The variation of $\overline{(\kappa_m^2)}_s \times \delta_{th}^2$ with $\widetilde{c}$ are shown in Fig. 11a for all the cases considered. It can be seen from Fig. 11a that $\overline{(\kappa_m^2)}_s \times \delta_{th}^2$ does not change significantly within the flame brush (i.e. for changing isosurface of reaction progress variable) for small turbulence intensities, whereas there is a slight increase in the values of $\overline{(\kappa_m^2)}_s \times \delta_{th}^2$ at the leading edge for the cases with high turbulence intensities, but in general the values for $\overline{(\kappa_m^2)}_s \times \delta_{th}^2$ do not vary significantly past $\widetilde{c} \geq 0.4$ for all the flames considered in this work. Thus the variation of $\overline{(\kappa_m^2)}_s \times \delta_{th}^2$ at $\widetilde{c} = 0.5$ with u'/S_L is exemplarily shown in Fig. 11b, which indicates that $\overline{(\kappa_m^2)}_s \times \delta_{th}^2$ increases with increasing u'/S_L but $\overline{(\kappa_m^2)}_s \times \delta_{th}^2$ does not change appreciably for large values of u'/S_L. The maximum possible value of $\overline{(\kappa_m^2)}_s$ can be scaled as $\overline{(\kappa_m^2)}_s \sim 1/\eta_c^2$ where η_c is the inner cut-off scale because the flame structures leading to $\overline{(\kappa_m^2)}_s > 1/\eta_c^2$ are expected to be annihilated due to the smoothing of highly curved surfaces by molecular diffusion effects (Yu & Lipatnikov, 2017). A number

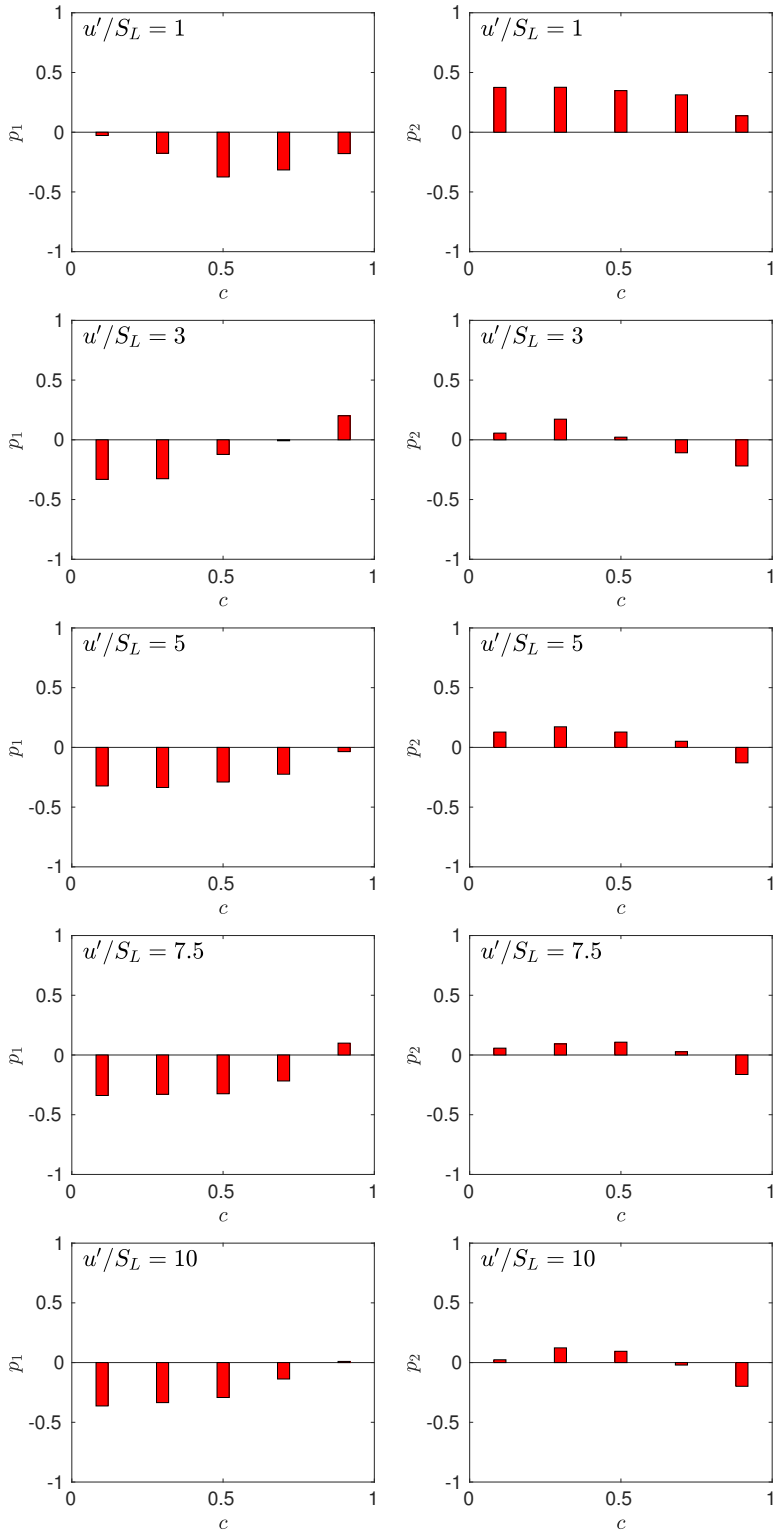

Figure 9.: Correlation coefficients between $(S_r + S_n)$ and κ_m (denoted by p_1), and between $|\nabla c|$ and κ_m (denoted by p_2) for different c values across the flame for all cases considered.

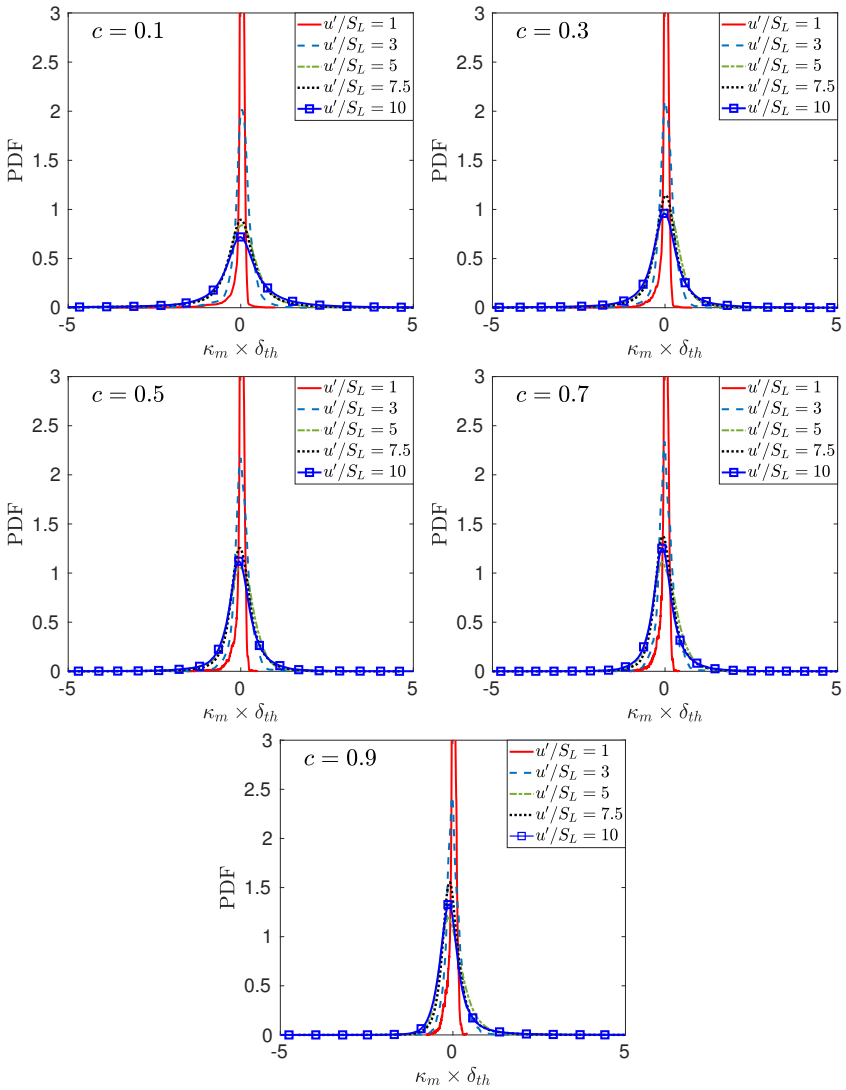

Figure 10.: PDFs of $\kappa_m \times \delta_{th}$ for different c values across the flame for all cases considered.

of previous analyses (Ahmed et al., 2018; Chakraborty & Klein, 2008b; Doan et al., 2017; Dunstan et al., 2013; Gao et al., 2014; Katragadda et al., 2012; Knikker et al., 2002) suggested η_c remains of the order of the thermal flame thickness. It can be seen from Fig. 11b that the largest magnitude of $\overline{(\kappa_m^2)}_s \times \delta_{th}^2$ within the flame brush indeed remains of the order of unity (i.e. $\overline{(\kappa_m^2)}_s \times \delta_{th}^2 \sim \mathcal{O}(1)$) for large values of u'/S_L. This, in turn, leads to the bending in T_{42V} and T_{4V} variation with u'/S_L. This finding for T_{42V} is consistent with that of Yu and Lipatnikov (2017) for a reaction wave in constant density forced isotropic turbulence; where it was shown that the small scale turbulent eddies become inefficient in wrinkling the reaction zone surface at high values of u'/S_L

as the small scale wrinkles are smoothed out by molecular transport. The similarity of the results between the present analysis and previous studies with constant density (Yu et al., 2015; Yu & Lipatnikov, 2017) implies that variable-density effects might be of secondary importance as far as physical mechanisms that control the bending effect are concerned.

The inner cut-off scale can be estimated by using the band pass filtering technique proposed by Leung et al. (2012). The bandpass filtering method used here suppresses eddies smaller or larger than L, and thus the flame stretch induced by eddies of size L can be extracted. This technique has been used in many previous analysis of reacting (Ahmed et al., 2018; Doan et al., 2017)) and non-reacting (Leung et al., 2012) flows. The bandpass filtering technique is used to determine the tangential strain contribution for eddies of scale L_s via $a_T^{L_s} = (\delta_{ij} - n_i n_j) S_{ij}^{L_s}$ and its surface averaged value is determined as :

$$\psi\left(L_s^+\right) = \left\langle \left|\nabla c\right| a_T^{L_s^+} \right\rangle / \left\langle \nabla c \right\rangle, \tag{11}$$

where $L_s^+ = L_s/\delta_{th}$ and $\psi_{int} = \int_0^\infty \psi dL_s^+$ gives the surface-averaged contributions from all the eddies contained in the flow. The cut-off scale η_c is estimated as l_{10}^+, where l_{10}^+ corresponds to the length scale at $\psi^* = 0.1$ ($\psi^* = \int_0^{L_s^+} \hat{\psi} dL_s^+$). The eddies smaller than l_{10}^+ contribute less than 10% or smaller to the total tangential strain rate experienced by the flame. Figure 12 shows the cut off scale obtained by the aforementioned analysis and demonstrates that η_c indeed remains of the order of δ_{th} for all cases but decreases with increasing u'/S_L. Moreover, η_c does not vary significantly in response to the changes in u'/S_L for large turbulence intensities. It can be observed by comparing figures 11b and 12 that $\overline{(\kappa_m^2)}_s \sim 1/\eta_c^2$ for the flames being investigated. A qualitatively similar result for the inner cut-off scale is obtained if it is evaluated using the FSD curvature term T_4 instead of the tangential strain rate term, and thus is not explicitly shown here for the sake of conciseness.

The current findings suggest that the inner cut-off scale η_c in the corrugated flamelets and thin reaction zones regime flames considered here is limited by the thermal flame thickness δ_{th}. Peters (2000) argued that the inner cut-off scale η_c scales

with the Gibson length scale $l_G \sim \delta_{th} Ka^{-2}$ in the corrugated flamelets regime (i.e. $Ka < 1$) and with Kolmogorov length scale $\eta \sim \delta_{th} Ka^{-0.5}$ in the thin reaction zones regime (i.e. $Ka > 1$). Although DNS based findings of Chakraborty and Klein (2008a) seemed to confirm the modelling arguments of Peters (2000), the inner cut-off scale η_c also scales with the thermal flame thickness δ_{th} for both corrugated and thin reaction zones regimes of premixed turbulent combustion. Moreover, a number of DNS (Ahmed et al., 2018; Chakraborty & Klein, 2008a; Doan et al., 2017; Dunstan et al., 2013; Gao et al., 2014; Katragadda et al., 2012) and experimental (Knikker et al., 2002) studies demonstrated that the inner cut-off scale indeed scales with thermal flame thickness even for the flames representing the thin reaction zones regime. It is worth noting that δ_{th} is defined based on the steepest temperature gradient but it remains greater than the physical length scale over which c changes from 0 to 0.6 (representing the pre-heat zone for the present thermo-chemistry). For a flame wrinkle with a characteristic length scale smaller than δ_{th}, nearby wrinkled flame elements are expected to interact with each other and molecular effects eventually smoothen them (Yu & Lipatnikov, 2017). However, further analyses with large length scale separation between l and δ_{th} will be needed for a conclusive proof. This is beyond the scope of this analysis and thus will not be discussed further in this paper.

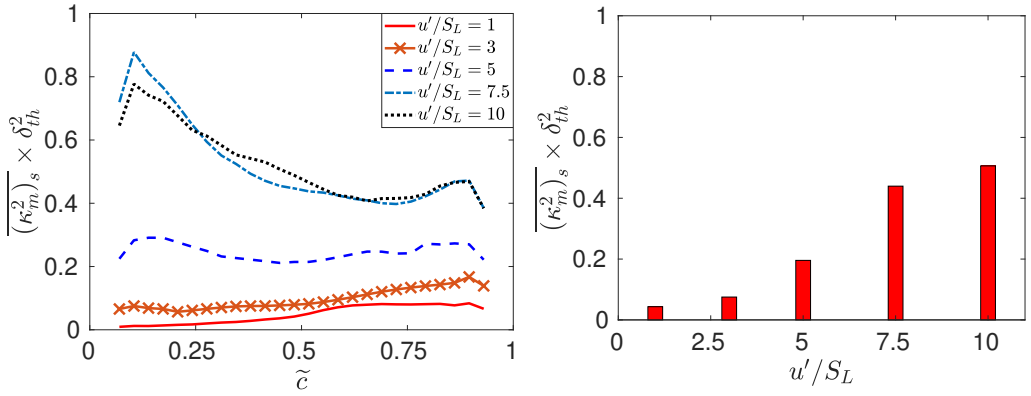

(a) (b)

Figure 11.: (a) Variation of $\overline{(\kappa_m^2)_s} \times \delta_{th}^2$ with $\widetilde{c}$ across the flame brush, (b) variation of $\overline{(\kappa_m^2)_s} \times \delta_{th}^2$ at $\widetilde{c} = 0.5$ with u'/S_L for all cases considered.

From the foregoing it can be concluded that the maximum possible magnitude of T_{42V} is driven by the maximum possible value of $\overline{(\kappa_m^2)_s}$. Thus, the negative value of the

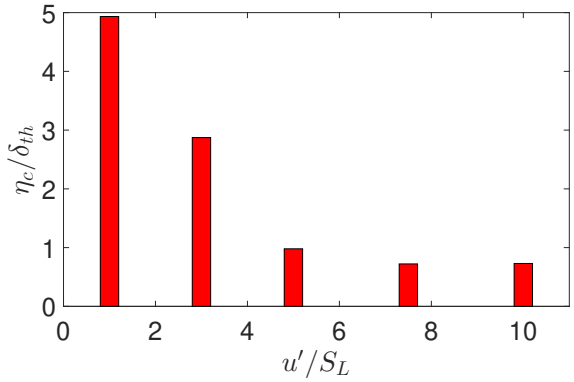

Figure 12.: Variations of inner cut-off scale η_c/δ_{th} for all cases considered.

FSD curvature term has an upper limit because the behaviour of T_{4V} is principally driven by $|T_{42V}| \propto \overline{(\kappa_m^2)}_s$ for large values of u'/S_L. This further indicates that the positive contribution by the tangential strain rate term has an upper limit because T_{2V} has to balance T_{4V} under quasi-steady state. Thus, an increase in turbulent straining does not indefinitely increase flame surface area because eventually small-scale wrinkles with characteristic length scales smaller than the inner cut-off scale are smoothed out by molecular diffusion effects (Yu & Lipatnikov, 2017). This indicates that the flame surface area generation by turbulent straining is countered and for steady state conditions nullified by the flame area destruction. The steady state balance of T_{2V} and T_{4V} itself is not sufficient for bending phenomenon. As both T_{2V} and T_{4V} do not increase indefinitely with increasing u'/S_L and show bending behaviours individually, and $\overline{(\kappa_m^2)}_s \times \delta_{th}^2$ saturates to a value of the order of unity, the flame surface area also no longer varies significantly with increasing u'/S_L. This gives rise to the bending effect in A_T/A_L, which subsequently translates to the bending effect in S_T/S_L .

In case of the flames considered in this work, the value of l/δ_{th} remains unchanged and thus an increase in turbulence intensity leads to an increase in the extent of flame wrinkling for small values of u'/S_L even when the volume-integrated values of the FSD strain rate and curvature terms are in equilibrium. This leads to an increase in A_T/A_L for small values of u'/S_L before bending where A_T/A_L no longer increases rapidly with increasing u'/S_L. It is difficult to isolate the effects of different length scales in the turbulence spectrum on the overall flame wrinkling and flame surface area. The most energetic eddies are the integral scale eddies and in all cases considered

here, the integral length scale is kept the same by the nature of turbulence forcing in the unburned gas. However, integral eddies are not necessarily most effective in wrinkling the flame but they have longer lifetime than the small-scale eddies which are more effective in wrinkling the flames than large-scale eddies (Meneveau & Poinsot, 1991). The net effect of turbulence straining is thus not solely dependent on large-scale turbulence straining ($\sim u'/l$) but also on a quantity, which was referred to as the efficiency function Γ by Meneveau and Poinsot (1991). The efficiency function has been parameterised by unsteady flame-vortex interaction and has been reported to be a strong increasing function of $\tilde{k}^{3/2}/(\tilde{\epsilon}\delta_{th})$ and a weak function of $\sqrt{2\tilde{k}/3}/S_L$ (Meneveau & Poinsot, 1991) where $\tilde{k}$ is the turbulent kinetic energy and $\tilde{\epsilon}$ is its dissipation rate. As the flame brush thickens with increasing u'/S_L , the efficiency function Γ and local values of large-scale straining ($\sim \tilde{\epsilon}/\tilde{k}$) vary significantly within the flame brush for the cases with high u'/S_L (not shown here). Thus, for small values of u'/S_L, the whole flame brush experiences similar magnitudes of effective straining, whereas turbulent straining is less effective in wrinkling the whole flame brush for high values of u'/S_L (not shown here).

The extent of flame-flame interaction and the smoothing of highly curved surfaces due to molecular diffusion (Yu & Lipatnikov, 2017) increases and the thermochemical processes are significantly perturbed for very large values of Karlovitz number Ka which, in turn, affect both dilatation rate $\nabla.\overrightarrow{u}$ and displacement speed S_d statistics in such a way that the flame surface area may decrease with an increase in u'/S_L for high Karlovitz number flames. Furthermore, the change in ∇c alignment from the eigenvector associated with e_α to the eigenvector corresponding to e_γ depends on Damköhler number Da. Because of the involvement of the length scale ratio l/δ_{th} in both Da and Ka, the bending effect is expected to be dependent on l/δ_{th} , which has not been addressed in this analysis and will be investigated in the future.

5. Conclusions

The bending effect in the turbulent speed variation with turbulence intensity has been analysed based on a three-dimensional DNS database of statistically planar unity Lewis

number premixed flames under forced unburned gas turbulence. It has been found that the bending effect in the turbulent flame speed variation originates principally due to the bending effect in the variation of flame surface area with turbulence intensity as the Damköhler's first hypothesis remains reasonably valid for the cases considered in this work. Thus, the bending effect has been analysed here in terms of the evolution of generalised FSD because of its close relation with flame surface area.

The volume-integrated value of the tangential strain rate term in the FSD transport equation assumes positive values, whereas the volume-inegrated value of the FSD curvature term remains negative. Under statistically stationary state, the volume-integrated values of the positive tangential strain rate term contribution, and the negative FSD curvature term remain in equilibrium. However, the statistical behaviours of both the tangential strain rate and curvature terms change with increasing turbulence intensity. The dilatation rate contribution to the flame surface area generation remains positive for all turbulence intensities but this contribution per unit surface area decreases for large values of Karlovitz number due to the disturbance of thermochemical processes by energetic turbulent eddies penetrating into the flame. The reaction progress variable gradient aligns with the eigenvector associated with the most extensive principal strain rate for small values of u'/S_L , which acts to destory the flame surface area through the normal strain rate contribution to the FSD evolution. However, for large values of u'/S_L, the reaction progress variable gradient aligns with the eigenvector associated with the most compressive principal strain rate, which acts to generate the flame surface area.

The negative contribution of the volume-integrated FSD curvature term originating from the combined reaction and normal diffusion component of displacement speed remains comparable to the flame area destruction by the tangential diffusion component of displacement speed for small values of Karlovitz number (i.e. small values of u'/S_L for a given value of l/δ_{th}). By contrast, the tangential diffusion component of displacement speed plays the dominant role and determines the overall flame surface area destruction for high values of Karlovitz number. The FSD curvature term due to the tangential diffusion component of displacement speed is directly proportional to the surface averaged value of curvature κ_m^2 and its maximum value has been demon-

strated to be limited by the inner cut-off scale. This upper limit of $\overline{(\kappa_m^2)}_s$ restricts the maximum extent of the flame surface area destruction and thereby the maximum possible generation of flame surface area under statistically stationary state. These upper limits of flame surface area generation and destruction ultimately give rise to bending effects in the variations of flame area and turbulent flame speed with u'/S_L.

The present analysis has been carried out for a given value of integral length scale to flame thickness ratio l/δ_{th} but the physical mechanisms which affect the dilatation rate, normal strain rate and curvature contributions depend on Damköhler and Karlovitz numbers. Thus,the effects of l/δ_{th} on the bending phenomenon deserve further investigation. Furthermore, the stretch effects on $\overline{(\rho S_d)}_s$ plays a significant role in statistically curved and/or non-unity Lewis number flames, which is less evident in the statistically planar flames considered here. Some of these aforementioned gaps will be addressed in future analyses. Although the presence of detailed chemical mechanism is unlikely to modify the qualitative nature of any of the findings of this paper, the incorporation of multi-step chemical schemes will be needed for the sake of completeness.

Acknowledgements

The authors are grateful to EPSRC for financial support (grant: EP/P022286/1) and computational support from ARCHER (grant: EP/K025163/1), CIRRUS, Leibniz Supercomputing Centre (grant: pr69ga) and HPC facility at Newcastle University (ROCKET).

References

Abdel-Gayed, R. G., Al-Khishali, K. J., & Bradley, D. (1984). Turbulent Burning Velocities and Flame Straining in Explosions. *Proc. R. Soc. A Math. Phys. Eng. Sci.*, *391*(1801), 393–414.

Abdel-Gayed, R. G., & Bradley, D. (1977). Dependence of turbulent burning velocity on turbulent reynolds number and ratio of flaminar burning velocity to R.M.S. turbulent velocity. *Symp. Combust.*, *16*(1), 1725–1735.

Ahmed, U., Doan, N. A. K., Lai, J., Klein, M., Chakraborty, N., & Swaminathan, N. (2018). Multiscale analysis of head-on quenching premixed turbulent flames. *Phys. Fluids*, *30*(10), 105102.

Ahmed, U., & Prosser, R. (2016, jan). Modelling flame turbulence interaction in RANS simulation of premixed turbulent combustion. *Combust. Theory Model.*, *20*(1), 34–57.

Ahmed, U., & Prosser, R. (2018). A Posteriori Assessment of Algebraic Scalar Dissipation Models for RANS Simulation of Premixed Turbulent Combustion. *Flow, Turbul. Combust.*, *100*(1), 39–73.

Ahmed, U., Prosser, R., & Revell, A. J. (2014). Towards the development of an evolution equation for flame turbulence interaction in premixed turbulent combustion. *Flow, Turbul. Combust.*, *93*(4), 637–663.

Aspden, A. J., Day, M. S., & Bell, J. B. (2011, may). Turbulenceflame interactions in lean premixed hydrogen: transition to the distributed burning regime. *J. Fluid Mech.*, *680*, 287–320.

Boger, M., Veynante, D., Boughanem, H., & Trouvé, A. (1998). Direct numerical simulation analysis of flame surface density concept for large eddy simulation of turbulent premixed combustion. *Symp. Combust.*, *27*(1), 917–925.

Bradley, D. (1992). How fast can we burn? *Symp. Combust.*, *24*(1), 247–262.

Bradley, D. (2002). Problems of predicting turbulent burning rates. *Combust. Theory Model.*, *6*(2), 361–382.

Bray, K. N. C. (1990, nov). Studies of the Turbulent Burning Velocity. *Proc. R. Soc. A Math. Phys. Eng. Sci.*, *431*(1882), 315–335.

Bray, K. N. C., & Cant, R. S. (1991, jul). Some Applications of Kolmogorov's Turbulence Research in the Field of Combustion. *Proc. R. Soc. A Math. Phys. Eng. Sci.*, *434*(1890), 217–240.

Butz, D., Gao, Y., Kempf, A. M., & Chakraborty, N. (2015). Large Eddy Simulations of a turbulent premixed swirl flame using an algebraic scalar dissipation rate closure. *Combust. Flame*, *162*(9), 3180–3196.

Candel, S. M., & Poinsot, T. J. (1990). Flame Stretch and the Balance Equation for the Flame Area. *Combust. Sci. Technol.*, *70*(1-3), 1–15.

Chakraborty, N., Alwazzan, D., Klein, M., & Cant, R. S. (2019, jul). On the validity of Damköhler's first hypothesis in turbulent Bunsen burner flames: A computational analysis. *Proc. Combust. Inst.*, *000*, 1–9.

Chakraborty, N., & Cant, R. S. (2004, apr). Unsteady effects of strain rate and curvature on turbulent premixed flames in an inflow-outflow configuration. *Combust. Flame*, *137*(1-2), 129–147.

Chakraborty, N., & Cant, R. S. (2005). Effects of strain rate and curvature on surface density function transport in turbulent premixed flames in the thin reaction zones regime. *Phys. Fluids*, *17*(6), 065108.

Chakraborty, N., & Cant, R. S. (2007). A priori analysis of the curvature and propagation terms of the flame surface density transport equation for large eddy simulation. *Phys. Fluids*, *19*(10).

Chakraborty, N., & Cant, R. S. (2009). Direct Numerical Simulation analysis of the Flame Surface Density transport equation in the context of Large Eddy Simulation. *Proc. Combust. Inst.*, *32*(1), 1445–1453.

Chakraborty, N., & Cant, R. S. (2011, sep). Effects of Lewis number on flame surface density transport in turbulent premixed combustion. *Combust. Flame*, *158*(9), 1768–1787.

Chakraborty, N., & Klein, M. (2008a, jun). Influence of Lewis number on the surface density function transport in the thin reaction zone regime for turbulent premixed flames. *Phys. Fluids*, *20*(6), 065102.

Chakraborty, N., & Klein, M. (2008b, aug). A priori direct numerical simulation assessment of algebraic flame surface density models for turbulent premixed flames in the context of large eddy simulation. *Phys. Fluids*, *20*(8), 085108.

Chakraborty, N., Klein, M., & Cant, R. S. (2007). Stretch rate effects on displacement speed in turbulent premixed flame kernels in the thin reaction zones regime. *Proc. Combust. Inst.*, *31 I*(1), 1385–1392.

Chakraborty, N., Klein, M., & Swaminathan, N. (2009). Effects of Lewis number on the reactive scalar gradient alignment with local strain rate in turbulent premixed flames. *Proc. Combust. Inst.*, *32 I*(1), 1409–1417.

Chakraborty, N., & Swaminathan, N. (2007). Influence of the Damköhler number on turbulence-scalar interaction in premixed flames. I. Physical insight. *Phys. Fluids*, *19*(4), 045103.

Chatakonda, O., Hawkes, E. R., Aspden, A. J., Kerstein, A. R., Kolla, H., & Chen, J. H. (2013). On the fractal characteristics of low Damköhler number flames. *Combust. Flame*, *160*(11), 2422–2433.

Damköhler, G. (1940). Der einfluss der turbulenz auf die flammengeschwindigkeit in gasgemis-

chen. *Zeitschrift für Elektrochemie und Angew. Phys. Chemie*, *46*(11), 601–626.

Doan, N., Swaminathan, N., & Chakraborty, N. (2017). Multiscale analysis of turbulence-flame interaction in premixed flames. *Proc. Combust. Inst.*, *36*(2), 1929–1935.

Dong, H. Q., Robin, V., Mura, A., & Champion, M. (2013). Analysis of algebraic closures of the mean scalar dissipation rate of the progress variable applied to stagnating turbulent flames. *Flow, Turbul. Combust.*, *90*(2), 301–323.

Dunstan, T. D., Minamoto, Y., Chakraborty, N., & Swaminathan, N. (2013). Scalar dissipation rate modelling for large eddy simulation of turbulent premixed flames. *Proc. Combust. Inst.*, *34*(1), 1193–1201. Retrieved from `http://dx.doi.org/10.1016/j.proci.2012.06.143`

Echekki, T., & Chen, J. H. (1999, jul). Analysis of the contribution of curvature to premixed flame propagation. *Combust. Flame*, *118*(1-2), 308–311.

Gao, Y., Chakraborty, N., & Swaminathan, N. (2014). Algebraic closure of scalar dissipation rate for large eddy simulations of turbulent premixed combustion. *Combust. Sci. Technol.*, *186*(10-11), 1309–1337.

Hawkes, E. R., & Cant, R. S. (2001, aug). Implications of a flame surface density approach to large eddy simulation of premixed turbulent combustion. *Combust. Flame*, *126*(3), 1617–1629.

Hawkes, E. R., & Chen, J. H. (2005). Evaluation of models for flame stretch due to curvature in the thin reaction zones regime. *Proc. Combust. Inst.*, *30*(1), 647–655.

Jenkins, K., & Cant, R. (1999). Direct numerical simulation of turbulent flame kernels. In D. Knight & L. Sakell (Eds.), *Recent advances in dns and les: Proceedings of the second afosr conference, rutgers - the state university of new jersey, new brunswick, usa* (pp. 191–202). Kluwer, Dordrecht.

Karpov, V., & Sokolik, A. (1961). The relationship between the self-inflammation of paraffins and their rates of laminar and turbulent burning. *Inst. Chem. Phys. USSR Acad. Sci. Moscow*, *138*, 874–876.

Katragadda, M., Chakraborty, N., & Cant, R. S. (2012). Effects of turbulent reynolds number on the performance of algebraic flame surface density models for large eddy simulation in the thin reaction zones regime: A direct numerical simulation analysis. *J. Combust.*, *2012*(2).

Katragadda, M., Malkeson, S. P., & Chakraborty, N. (2011). Modelling of the tangential strain rate term of the Flame Surface Density transport equation in the context of Reynolds Averaged NavierStokes simulation. *Proc. Combust. Inst.*, *33*(1), 1429–1437.

Katragadda, M., Malkeson, S. P., & Chakraborty, N. (2014). Modelling of the curvature

term in the flame surface density transport equation : a direct numerical simulations based analysis. *Int. J. spray Combust. Dyn.*, *6*(2), 163–198.

Kim, H. S., & Pitsch, H. (2007). Scalar gradient and small-scale structure in turbulent premixed combustion. *Phys. Fluids*, *19*(11).

Klein, M., Chakraborty, N., & Ketterl, S. (2017, dec). A Comparison of Strategies for Direct Numerical Simulation of Turbulence Chemistry Interaction in Generic Planar Turbulent Premixed Flames. *Flow, Turbul. Combust.*, *99*(3-4), 955–971.

Knikker, R., Veynante, D., & Meneveau, C. (2002). A priori testing of a similarity model for large eddy simulations of turbulent premixed combustion. *Proceeding Combust. Inst.*, *29*, 2105–2111.

Leung, T., Swaminathan, N., & Davidson, P. A. (2012). Geometry and interaction of structures in homogeneous isotropic turbulence. *J. Fluid Mech.*, *710*, 453–481.

Lipatnikov, A. N., & Chomiak, J. (2002). Turbulent flame speed and thickness: Phenomenology, evaluation, and application in multi-dimensional simulations. *Prog. Energy Combust. Sci.*, *28*(1), 1–74.

Lipatnikov, A. N., & Chomiak, J. (2005). Molecular transport effects on turbulent flame propagation and structure. *Prog. Energy Combust. Sci.*, *31*(1), 1–73.

Meneveau, C., & Poinsot, T. J. (1991). Stretching and quenching of flamelets in premixed turbulent combustion. *Combust. Flame*, *332*, 311–332.

Nivarti, G. V., & Cant, R. S. (2017a). Direct Numerical Simulation of the bending effect in turbulent premixed flames. *Proc. Combust. Inst.*, *36*(2), 1903–1910.

Nivarti, G. V., & Cant, R. S. (2017b, aug). Scalar transport and the validity of Damköhler's hypotheses for flame propagation in intense turbulence. *Phys. Fluids*, *29*(8), 085107.

Peters, N. (2000). *Turbulent Combustion*. Cambridge University Press.

Peters, N., Terhoeven, P., Chen, J. H., & Echekki, T. (1998). Statistics of flame displacement speeds from computations of 2-D unsteady methane-air flames. *Symp. Combust.*, *27*(1), 833–839.

Poinsot, T. J., & Lele, S. (1992, jul). Boundary conditions for direct simulations of compressible viscous flows. *J. Comput. Phys.*, *101*(1), 104–129.

Pope, S. B. (1988). The evolution of surfaces in turbulence. *Int. J. Eng. Sci.*, *26*(5), 445–469.

Sabelnikov, V. A., Lipatnikov, A. N., Chakraborty, N., Nishiki, S., & Hasegawa, T. (2017). A balance equation for the mean rate of product creation in premixed turbulent flames. *Proc. Combust. Inst.*, *36*(2), 1893–1901.

Sellmann, J., Lai, J., Kempf, A. M., & Chakraborty, N. (2017). Flame surface density based modelling of head-on quenching of turbulent premixed flames. *Proc. Combust. Inst.*, *36*(2), 1817–1825.

Trouvé, A., & Poinsot, T. (1994, nov). The evolution equation for the flame surface density in turbulent premixed combustion. *J. Fluid Mech.*, *278*, 1–31.

Veynante, D., Trouvé, A., Bray, K. N. C., & Mantel, T. (1997, feb). Gradient and counter-gradient scalar transport in turbulent premixed flames. *J. Fluid Mech.*, *332*, 263–293.

Wacks, D. H., Chakraborty, N., Klein, M., Arias, P. G., & Im, H. G. (2016). Flow topologies in different regimes of premixed turbulent combustion: A direct numerical simulation analysis. *Phys. Rev. Fluids*, *1*(8), 1–16.

Wray, A. A. (1990). *Minimal storage time advancement schemes for spectral methods* (Tech. Rep.). Report No. MS 202 A-1, NASA Ames Research Center, California, USA.

Yu, R., Bai, X.-S., & Lipatnikov, A. N. (2015, jun). A direct numerical simulation study of interface propagation in homogeneous turbulence. *J. Fluid Mech.*, *772*, 127–164.

Yu, R., & Lipatnikov, A. N. (2017, jun). Direct numerical simulation study of statistically stationary propagation of a reaction wave in homogeneous turbulence. *Phys. Rev. E*, *95*(6), 063101.

Zhang, S., & Rutland, C. J. (1995, sep). Premixed flame effects on turbulence and pressure-related terms. *Combust. Flame*, *102*(4), 447–461.